16th World Congress in Computational Mechanics (WCCM)
21-26 July 2024, Vancouver, Canada
A. Korobenko, M. Laforest, S. Prudhomme, R. Vaziri (Eds)

THREE-FIELD MODEL FOR WAVE PROPAGATION IN POROUS MEDIA BASED ON MIXTURE THEORY

BRUNA CAMPOS[1], **ROBERT GRACIE**[1]

[1] University of Waterloo
N2L 3G1
bccampos@uwaterloo.ca

[2] University of Waterloo
N2L 3G1
rgracie@uwaterloo.ca

Key words: Porous media, FEM, wave propagation, mixture theory, three-field formulation.

Abstract. Simulations of wave propagation in porous media are important to the understanding of various phenomena, such as seismic effects and non-destructive testing. The derivation and implementation of finite element analysis for a fully dynamic three-field deformable porous media model based on the de la Cruz and Spanos (dCS) theory [1] is presented. The dCS theory accounts for the fluid viscous dissipation mechanism and nonreciprocal solid-fluid interactions, which are neglected in Biot theory [2]. While the Biot theory is based on experimental data, the dCS theory is derived from mixture theories associated with the volume fraction concept and representing the connection between micro and macro pore scales. dCS results presented build upon recent FE model for quasi-static analysis [3]. Here, for the fully dynamic case incorporating both fluid and solid inertia, the accuracy and robustness of the FEA model is verified by wave propagation examples in one and two dimensions. Time integration scheme utilized and the changes in convergence rates according to how strongly coupled is the system will be discussed. The required element approximation order for all variables to ensure numerical stability will be demonstrated. The presented model is compared with the results from Biot theory, allowing one to observe the differences between the two theories and their relevance. The solutions in the time and frequency domain are also discussed, where the analysis of the correspondent eigenproblem leads to important information regarding wave velocity and attenuation.

1 INTRODUCTION

The Biot (BT) theory is one of the first porous media theories developed [4]. It represents the solid and fluid components, as well as their interaction, through a coupled set of governing equations. Applications of the BT theory can be found for instance in quasi-static soil consolidation [5], wave propagation [6], and non-destructive testing [7]. BT theory assumes that there

is a unique potential deformation energy related to the porous medium, and hence solid and fluid are assumed to deform to the same extent [8]. More to that, the BT formulation neglects the fluid viscous dissipation terms present in the fluid stress definition. Consequently, it yields the representation of only three wave types: a fast P, a slow P, and a fast S wave, hence neglecting a slow S wave [9].

Following the development of the BT theory, other porous media theories based on mixture theory and the volume fraction concept were proposed [10]. They assume that the porous media governing equations are valid at the micro-scale, and volume-averaging techniques are applied to extend them to the macro-scale. In this process, porosity is taken as a field variable. One example is the de la Cruz and Spanos (dCS) theory [11, 12]. In the dCS framework, besides including porosity as a variable, it also includes fluid viscous dissipation terms that were previously neglected in the BT model [13]. Later developments of the dCS model also accounted for non-reciprocal solid-fluid interactions, which happen when the constituents deform to different extents [14].

The use of numerical models to simulate porous media behavior has been vast throughout the years, and various choices of main variables have been adopted. Two-field porous media formulations, for instance, are written in terms of solid displacement and fluid pressure [15, 16]. Three-field models, on the other hand, can have solid displacement, fluid pressure, and fluid displacement as main variables [17, 18]. Recently, the authors derived a finite element (FE) model for a quasi-static dCS model [3]. Building upon such results, this work presents a finite element model for the simulation of dynamic problems in the dCS context. The dCS FE model is verified against a manufactured solution, and a convergence study is performed. Moreover, one- and two-dimensional examples are presented so that we can evaluate the impact of the fluid viscous dissipation terms and the non-reciprocal solid-fluid interactions. The dCS results are compared with the BT theory, when we observe how they might diverge depending on the problem characteristics.

2 POROUS MEDIA GOVERNING EQUATIONS

Based on the dCS formulation presented in [1], and assuming an isothermal model, the solid and fluid equations of motion are

$$(1-\eta_0)\rho_s\ddot{\mathbf{u}}_s = \boldsymbol{\nabla}\cdot\boldsymbol{\sigma}_s + \frac{\mu_f\eta_0^2}{\kappa}(\dot{\mathbf{u}}_f - \dot{\mathbf{u}}_s) - \rho_{12}(\ddot{\mathbf{u}}_f - \ddot{\mathbf{u}}_s), \tag{1}$$

$$\eta_0\rho_f\ddot{\mathbf{u}}_f = \boldsymbol{\nabla}\cdot\boldsymbol{\sigma}_f - \frac{\mu_f\eta_0^2}{\kappa}(\dot{\mathbf{u}}_f - \dot{\mathbf{u}}_s) + \rho_{12}(\ddot{\mathbf{u}}_f - \ddot{\mathbf{u}}_s), \tag{2}$$

in which $\mathbf{u}_f, \mathbf{u}_s$ are fluid and solid displacements, respectively; η_0 is the initial porosity, ρ_s is the solid density, ρ_f is the fluid density, μ_f is the fluid dynamic viscosity, κ is the intrinsic permeability, and ρ_{12} is the added mass coefficient. The dots as superscripts indicate time derivatives: $\dot{\mathbf{u}}_f, \dot{\mathbf{u}}_s$ are velocities and $\ddot{\mathbf{u}}_f, \ddot{\mathbf{u}}_s$ are accelerations of the fluid and solid constituents. The divergence of solid and fluid stresses $\boldsymbol{\nabla}\cdot\boldsymbol{\sigma}_s$, $\boldsymbol{\nabla}\cdot\boldsymbol{\sigma}_f$, are given by

$$\boldsymbol{\nabla}\cdot\boldsymbol{\sigma}_s = \quad (1-\eta_0)K_s - K_s\boldsymbol{\nabla}\eta + \mu_M[\boldsymbol{\nabla}^2\mathbf{u}_s + \frac{1}{3}\boldsymbol{\nabla}(\boldsymbol{\nabla}\cdot\mathbf{u}_s)], \tag{3}$$

$$\boldsymbol{\nabla}\cdot\boldsymbol{\sigma}_f = \quad -\eta_0\boldsymbol{\nabla}p + \eta_0\mu_f\boldsymbol{\nabla}^2\dot{\mathbf{u}}_f + \eta_0(\xi_f + \frac{\mu_f}{3})\boldsymbol{\nabla}(\boldsymbol{\nabla}\cdot\dot{\mathbf{u}}_f) + \xi_f\boldsymbol{\nabla}\dot{\eta}, \tag{4}$$

where p is the fluid pressure variable, K_s is the solid bulk modulus, ξ_f is the fluid bulk viscosity, $\mu_M = (1+c)(1-\eta_0)\mu_s$ is the macroscopic shear modulus, μ_s is the solid shear modulus, and c is a micro-heterogeneity parameter [1]. The storage equation is written as

$$\frac{\dot{p}}{K_f} + \boldsymbol{\nabla}\cdot\dot{\mathbf{u}}_f + \frac{\dot{\eta}}{\eta_0} = s, \tag{5}$$

in which K_f is the fluid bulk modulus, s is a source/sink term, and the porosity variable η is related to the solid and fluid displacements $\mathbf{u}_s$, $\mathbf{u}_f$ by

$$\dot{\eta} = \delta_s\boldsymbol{\nabla}\cdot\dot{\mathbf{u}}_s - \delta_f\dot{\mathbf{u}}_f. \tag{6}$$

In the porosity relation (6), δ_s, δ_f are compliance coefficients defined as [14]

$$\delta_s = (\alpha-\eta_0)\frac{\eta_0 M^*}{K_f}, \quad \delta_f = (\alpha-\eta_0)\frac{\eta_0 M^*}{K_s}n, \tag{7}$$

where α is the Biot coefficient, n is the porosity effective pressure coefficient, and the modified storage coefficient M^* is related to the Biot storage coefficient M by

$$\frac{1}{M^*} = \frac{1}{M} - (1-n)\frac{\alpha-\eta_0}{K_s}, \quad \frac{1}{M} = \frac{\alpha-\eta_0}{K_s} + \frac{\eta_0}{K_f}. \tag{8}$$

The compliance coefficients can be taken as weighting parameters for the solid and fluid deformations, representing their impact on the change in porosity. In this sense, variations in n can be associated with physical phenomena in the porous medium. When $n = 1$, solid and fluid constituents affect porosity to the same extent, and the formulation presented in Biot theory is recovered [14, 3]. At its lower bound, i.e., $n = 0$, fluid has no effect on porosity change. On the other hand, the upper bound $n = K_s/K_f$ leads to no variations in porosity. It is noteworthy that we have assumed that the macroscopic shear modulus μ_M is equal to the averaged solid shear modulus $(1-\eta_0)\mu_s$, meaning that the micro-heterogeneity parameter c is equal to zero [1]. While $c = 0$ (and $n = 1$) recovers the BT formulation, changes in c might lead to deviations from BT. Nevertheless, this study is out of the scope of the present work.

The system of equations to solve is written in terms of solid displacement $\mathbf{u}_s$, fluid pressure p, and fluid displacement $\mathbf{u}_f$,

$$\begin{cases} \boldsymbol{\nabla}\cdot\boldsymbol{\sigma} - (1-\eta_0)\rho_s\ddot{\mathbf{u}}_s + \eta_0\boldsymbol{\nabla}p - \eta_0\mu_f\boldsymbol{\nabla}^2\dot{\mathbf{u}}_f - \eta_0(\xi_f + \frac{\mu_f}{3})\boldsymbol{\nabla}(\boldsymbol{\nabla}\cdot\dot{\mathbf{u}}_f) \\ \qquad -\xi_f\delta_s\boldsymbol{\nabla}(\boldsymbol{\nabla}\cdot\dot{\mathbf{u}}_s) + \xi_f\delta_f\boldsymbol{\nabla}(\boldsymbol{\nabla}\cdot\dot{\mathbf{u}}_f) + \frac{\mu_f\eta_0^2}{\kappa}(\dot{\mathbf{u}}_f - \dot{\mathbf{u}}_s) - \rho_{12}(\ddot{\mathbf{u}}_f - \ddot{\mathbf{u}}_s) = 0, \\ \frac{p}{K_f} + \frac{\delta_s}{\eta_0}\boldsymbol{\nabla}\cdot\mathbf{u}_s + (1-\frac{\delta_f}{\eta_0})\boldsymbol{\nabla}\cdot\mathbf{u}_f = 0, \\ -\eta_0\rho_f\ddot{\mathbf{u}}_f - \eta_0\boldsymbol{\nabla}p + \eta_0\mu_f\boldsymbol{\nabla}^2\dot{\mathbf{u}}_f + \eta_0(\xi_f + \frac{\mu_f}{3})\boldsymbol{\nabla}(\boldsymbol{\nabla}\cdot\dot{\mathbf{u}}_f) + \xi_f\delta_s\boldsymbol{\nabla}(\boldsymbol{\nabla}\cdot\dot{\mathbf{u}}_s) \\ \qquad -\xi_f\delta_f\boldsymbol{\nabla}(\boldsymbol{\nabla}\cdot\dot{\mathbf{u}}_f) - \frac{\mu_f\eta_0^2}{\kappa}(\dot{\mathbf{u}}_f - \dot{\mathbf{u}}_s) + \rho_{12}(\ddot{\mathbf{u}}_f - \ddot{\mathbf{u}}_s) = 0; \end{cases} \tag{9}$$

the first equation is obtained by the summation of the solid and fluid equations of motion (1)-(2), where the total stress $\boldsymbol{\sigma}$ is given by $\boldsymbol{\sigma} = \boldsymbol{\sigma}_s + \boldsymbol{\sigma}_f$. The second equation comes from the integration of the storage equation (5) with respect to time. The third equation is the fluid equation of motion; in (9), the porosity variable was substituted by the relation expressed in (6).

3 FINITE ELEMENT DISCRETIZATION

After deriving the weak form, the system of equations (9) yields the finite element semi-discretized form

$$\mathbf{M}\ddot{\mathbf{d}} + \mathbf{C}\dot{\mathbf{d}} + \mathbf{K}\mathbf{d} = \mathbf{f}, \tag{10}$$

in which $\mathbf{M}$ is the mass matrix, $\mathbf{C}$ is the damping matrix, $\mathbf{K}$ is the stiffness matrix, $\mathbf{f}$ is the boundary term vector, and $\mathbf{d}$ is the vector of nodal values for solid displacement, fluid pressure, and fluid displacement. The submatrices in $\mathbf{M}$ are

$$\mathbf{M}_{ss} = [(1-\eta_0)\rho_s - \rho_{12}] \int_\Omega \mathbf{N}_s^\top \mathbf{N}_s d\Omega, \qquad \mathbf{M}_{sf} = \rho_{12} \int_\Omega \mathbf{N}_s^\top \mathbf{N}_f d\Omega,$$
$$\mathbf{M}_{ff} = [\eta_0\rho_f - \rho_{12}] \int_\Omega \mathbf{N}_f^\top \mathbf{N}_f d\Omega, \qquad \mathbf{M}_{fs} = \rho_{12} \int_\Omega \mathbf{N}_f^\top \mathbf{N}_s d\Omega;$$

the damping submatrices are

$$\mathbf{C}_{ss} = -\xi_f\delta_s \int_\Omega \mathbf{B}_s^\top \mathbf{B}_s d\Omega, \qquad \mathbf{C}_{ff} = (\frac{4}{3}\eta_0\mu_f + \eta_0\xi_f - \xi_f\delta_f) \int_\Omega \mathbf{B}_f^\top \mathbf{B}_f d\Omega,$$
$$\mathbf{C}_{sf} = -\xi_f\delta_s \int_\Omega \mathbf{B}_s^\top \mathbf{B}_f d\Omega, \qquad \mathbf{C}_{fs} = (\frac{4}{3}\eta_0\mu_f + \eta_0\xi_f - \xi_f\delta_f) \int_\Omega \mathbf{B}_f^\top \mathbf{B}_s d\Omega;$$

and the stiffness submatrices are

$$\mathbf{K}_{ss} = \int_\Omega \mathbf{B}_s^\top \mathbf{D}\mathbf{B}_s d\Omega, \qquad \mathbf{K}_{sp} = (\alpha - \eta_0) \int_\Omega \mathbf{B}_s^\top \mathbf{N}_p d\Omega,$$
$$\mathbf{K}_{ps} = \frac{\delta_s}{\eta_0} \int_\Omega \mathbf{N}_p^\top \mathbf{B}_s d\Omega, \qquad \mathbf{K}_{pp} = \frac{1}{K_f} \int_\Omega \mathbf{N}_p^\top \mathbf{N}_p d\Omega,$$
$$\mathbf{K}_{pf} = (1 - \frac{\delta_f}{\eta_0}) \int_\Omega \mathbf{N}_p^\top \mathbf{B}_f d\Omega, \qquad \mathbf{K}_{fp} = \eta_0 \int_\Omega \mathbf{B}_f^\top \mathbf{N}_p d\Omega.$$

For the fully discretized system, the generalized Newmark method [19] is employed for time integration. To introduce some sort of damping, the related time integration constants are taken as 0.7, and thus the method is first-order accurate in time.

4 NUMERICAL EXAMPLES

4.1 Verification and convergence study

A manufactured solution is used in a one-dimensional example for verification and convergence studies related to the proposed dCS FE model. The solid displacement, fluid pressure, and fluid displacement fields are given by

$$u_s = \frac{\sin(x+2t)}{1000}, \qquad p = \frac{\sin(x)+\sin(2t)}{1000}, \qquad u_f = \frac{\cos(x+2t)}{1000}. \tag{11}$$

The domain has a length of $L = 6$m; for the verification study, the mesh consists in $ne = 200$ elements with a quadratic approximation for the solid and fluid displacement fields, and a linear approximation for the fluid pressure field. The final simulation time is $t_{\text{end}} = 1$s with a time step of $\Delta t = 10^{-5}$s. The numerical results for all three fields match the chosen manufactured solution.

For the convergence study, the final simulation time and the time step are kept the same, and the element size is gradually decreased. The results for five different values of ne are plotted in Figure 1 alongside correspondent regression lines. The convergence rates for the three-field dCS model are $m = 2.17$ for the solid displacement, $m = 1.46$ for the fluid pressure, and $m = 1.95$ for the fluid displacement. As noticed, the reported rates differ from those obtained in uncoupled linear problems – order 2 for linear elements and order 3 for quadratic elements. This is due to the coupling nature of the problem, and the more strongly coupled the porous media simulation is, the more the convergence rates decrease.

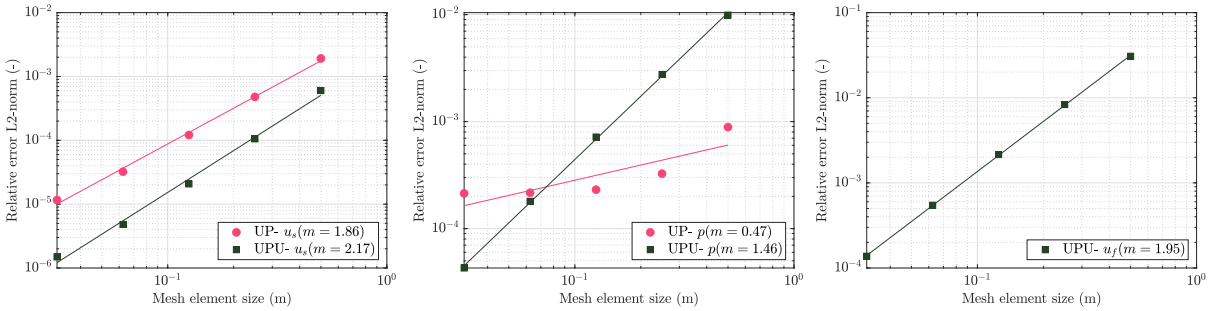

(a) u_s field (b) p field (c) u_f field

Figure 1: Relative error of L2-norm for the three-field dCS model; items (a) and (b) also include the convergence slopes for the two-field $u_s - p$ dCS model.

For comparison purposes, Figure 1 also depicts convergence rates for a two-field dCS model, having only solid displacement and fluid pressure as main variables. As noticed, the two-field model has poorer rates that the three-field model. This is an expected result; the two-field formulation assumes that solid and fluid accelerations are the same, and it is usually employed in only quasi-static simulations due to the consequent lack of accuracy in dynamic simulations.

4.2 Effect of fluid viscous dissipation

When the porosity effective pressure coefficient is taken as $n = 1$ and the micro-heterogeneity parameter is $c = 0$, the sole difference between the dCS and the BT models is the presence of fluid viscous dissipation terms in the former, as part of the fluid stress definition. In this section

we assume $n = 1$ and $c = 0$, and evaluate the effect of the viscous terms in the dCS theory for different porous media constituents. Such study is performed through an assessment of wave velocity and attenuation patterns in porous media. Whilst BT theory yields two P waves and one S wave, the dCS theory yields also an additional slow S wave due to the viscous dissipation terms. The new S wave might have an impact on the other wave types, which is also a topic of observation in this section.

Five solid-fluid combinations are considered (note that, in all cases, we assume that the medium is fully saturated): (M1) water and sandstone [20], (M2) water and cancellous bone tissue [21], (M3) fluidized snow and ice [22], (M4) brine and marine sediments [23], and (M5) heavy oil and marine sediments. Figures 2 and 3 depict the normalized velocity and attenuation values, respectively, of the four evaluated wave types for the BT and dCS models.

Results for the solid-fluid combinations M1, M3, and M4 are practically identical for both BT and dCS, hence attesting that viscous dissipation terms are negligible in these cases. More to that, the slow S wave is highly dissipative, showing a low velocity (specially at low frequencies) range between 0.10 m/s (M4) and 32 m/s (M3) and an attenuation range in the order of 10^3 to 10^6 for low frequencies.

The water-cancellous bone combination (M2) depicts few changes between BT and dCS models, where the only noticeable discrepancy appears in the first P wave attenuation, increasing by 30% in dCS. The slow P wave in this scenario is also characterized by low velocity and high attenuation. For the porous media M5, the solid constituent in combination M4 – marine sediments – is coupled with a very heavy oil. In this case, due to the high fluid viscosity, BT and dCS theories diverge. Differences in the results are more noticeable for the second P and first S waves, where velocity and attenuation in the dCS model is significantly higher.

4.3 Effect of non-reciprocal interactions

A two-dimensional example of wave propagation is used to evaluate the effect of non-reciprocal interactions included in the dCS framework. A water-saturated sandstone porous media is considered, for which the adopted material parameters [13] are listed in Table 1. The square domain has dimensions of $L = 12$m, and a wave source $s_w(t)$ of the form

$$s_w(t) = P_0 \left(\sin(\pi t f) - 0.5 \sin(2\pi t f)\right), t < 1/f \tag{12}$$

is applied at the center of the domain ($x = 6$m, $y = 6$m). In this wave source equation, t is the time variable, $P_0 = 10^5$Pa is the source amplitude, and $f = 10^3$Hz is the source frequency. The domain is discretized into a mesh with 240×240 quadrilateral elements. A bi-linear approximation is employed for all three variable fields. The final simulation time is taken as $t_{\text{end}} = 2 \times 10^{-3}$s with a time step of $\Delta t = 10^{-5}$s.

Figure 4 shows the solid displacement, fluid pressure, and fluid displacement distribution over the domain at the final simulation time for the dCS model herein presented. As depicted in Figure 5, it is possible to identify the propagation of the first P wave and the first S wave. Due to the high attenuation of the slow P and S waves, they could not be identified within the context of this example. Figure 6 depicts the variation in the same fields, now comparing variations in

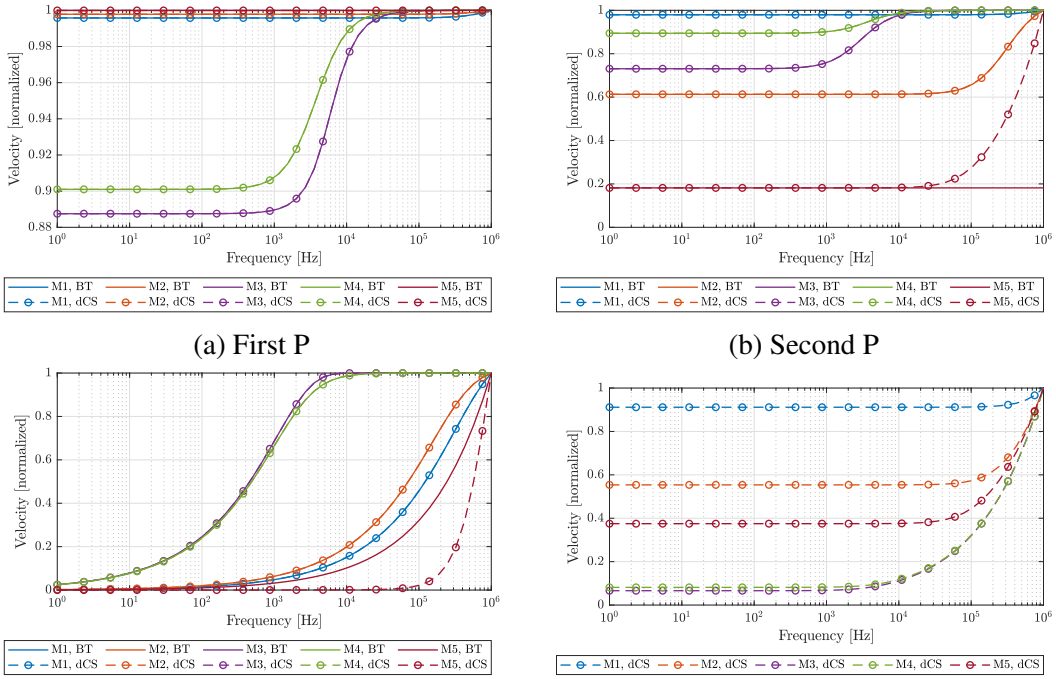

(a) First P

(b) Second P

(c) First S

(d) Second S

Figure 2: Wave velocity for different materials considering both BT and dCS models.

Table 1: Material parameters for two-dimensional wave propagation considering water-saturated sandstone constituents [13].

Parameter	Value	Unit	Parameter	Value	Unit
E	11.76	GPa	K_s	33	GPa
ν	0.2	-	K_f	2.2	GPa
κ	1×10^{-13}	m^2	ρ_s	2650	kg/m^3
α	0.78	-	ρ_f	1000	kg/m^3
η_0	0.25	-	ρ_{12}	0	kg/m^3
μ_f	10^{-3}	Pa · s	$\delta_s(n=1)$	0.4644	-
ξ_f	2.8×10^{-3}	Pa · s	$\delta_f(n=1)$	0.0310	-

the non-reciprocity in dCS framework with BT theory results. We notice that when the porosity effective pressure coefficient is equal to 1, dCS and BT results coincide. The only difference between dCS and BT theories in this case is the additional fluid viscous dissipation terms in the former. Hence, such terms are negligible for the specific conditions – material parameters, amplitude and frequency of the wave source – of this example.

When $n = n_{\text{min}}$, we notice a slight increase in attenuation of the solid velocity, and a slight

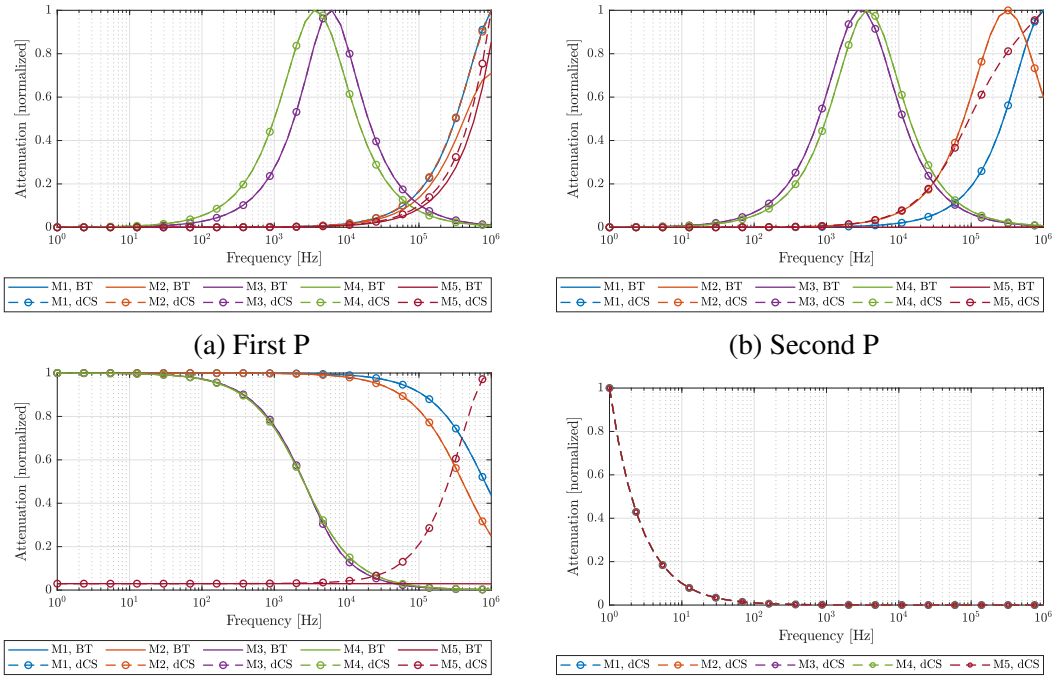

(a) First P

(b) Second P

(c) First S

(d) Second S

Figure 3: Wave attenuation for different materials considering both BT and dCS models.

decrease in attenuation for the fluid pressure when compared to $n = 1$. The wave velocity, on the other hand, is very similar to when $n = 1$. For $n = n_{\text{max}}$, changes are more significant, and now there is less attenuation in the solid velocity and more attenuation in the fluid pressure field; wave velocity also seems to change in this case. Variations in wave behavior can be explained by the significance of the porosity effective pressure coefficient n. It is used to indicate the presence of heterogeneity, being related to the concentration of potential energy in the solid/fluid constituents or at their interface. A more detailed explanation of its meaning can be found in [14].

5 DISCUSSION

The robustness of dCS finite element model herein proposed was verified by using a manufactured solution in a one-dimensional case. The Newmark method was used for the time integration, in which the related constants were assumed in a way such that some numerical damping is added to the problem. Further analysis showed that the absence of such damping lead to numerical instabilities. Optimal convergence rates were obtained, and we observed how these rates are superior than those of a two-field dCS model. This happens due to the fact that a two-field formulation can only be obtained under the assumption that solid and fluid accelerations are equal, which reduces the model accuracy when dealing with dynamic simulations. Moreover, additional tests confirmed that the adopted material parameters influence on the mesh

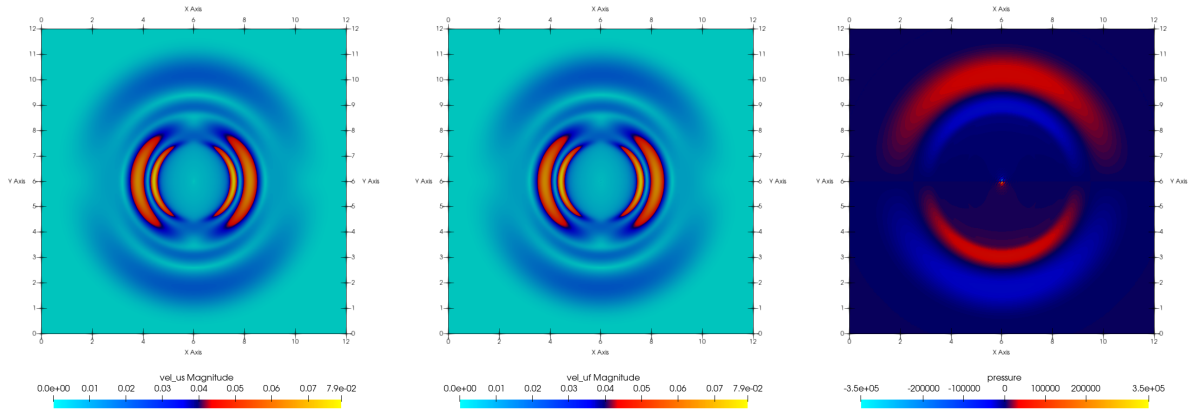

(a) Solid velocity [m/s] (b) Fluid velocity [m/s] (c) Fluid pressure [Pa]

Figure 4: Wave propagation in two-dimensional domain.

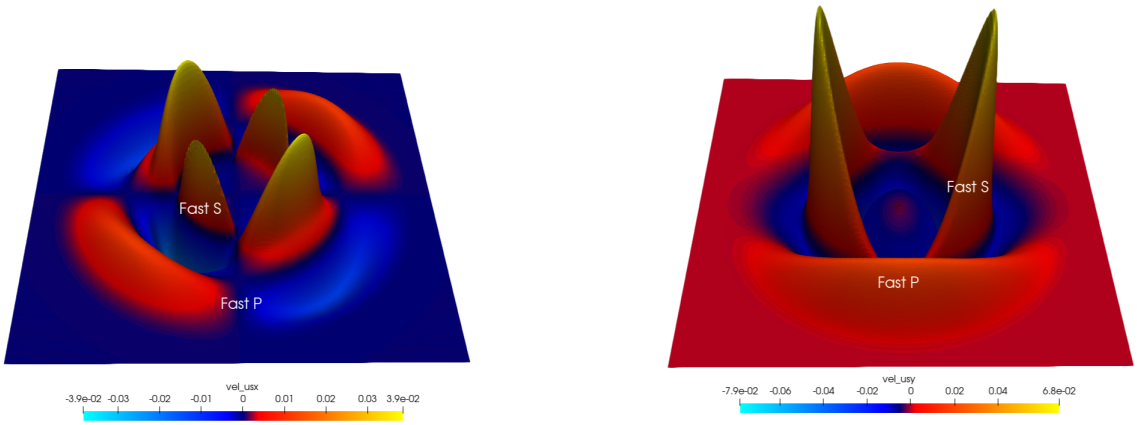

(a) Solid velocity in x [m/s] (b) Solid velocity in y [m/s]

Figure 5: Solid velocity for the two-dimensional wave propagation.

size convergence rates. At the limit where the porous medium coupling terms vanish, the convergence rates from uncoupled problems were recovered. Therefore, we can conclude that the slope of convergence is directly related to how strongly coupled the solid and fluid constituents are.

A one-dimensional example was considered to study the effect of the fluid viscous dissipation terms present in the dCS model (and neglected in the BT theory). Five different solid-fluid combinations were observed. The analysis considered the eigenproblem related to the dCS wave equations, which lead to expressions for phase velocity and attenuation. Differences between wave velocity and attenuation for the BT and dCS models appeared at high frequencies, and were more significant when the fluid had high viscosity. It is noteworthy, hence, that while

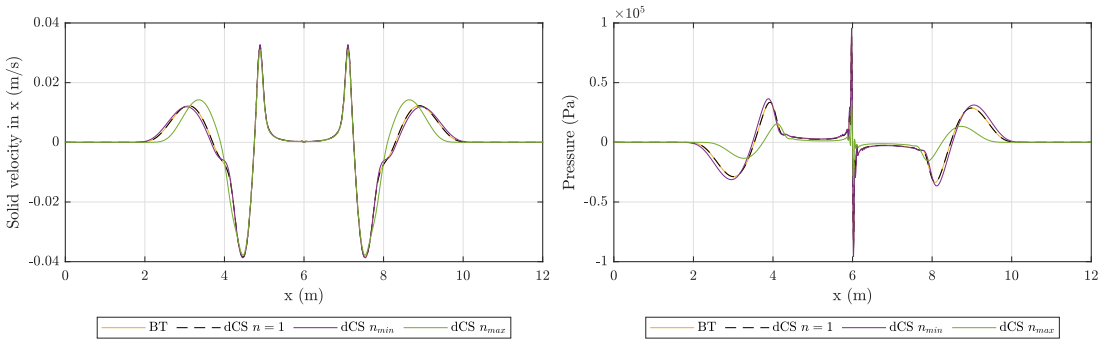

(a) Solid velocity in x [m/s] (b) Fluid pressure [Pa]

Figure 6: Comparison between BT and dCS results for the two-dimensional wave propagation, considering variations in the coefficient n for the dCS model.

dCS theory matches BT results in various situations, it might better represent wave patterns for certain combinations of solid-fluid constituents.

Wave propagation was represented in a two-dimensional domain, where we evaluated the impact of non-reciprocal solid-fluid interactions. It was noted that changes in n affect both the wave velocity and attenuation in the medium. Furthermore, the propagation of both fast P and fast S waves were identified. Due to the dissipative characteristic of the slow P and S waves, they could not be observed. While the one-dimensional examples considered mixed-order elements, the two-dimensional wave propagation was simulated considering bi-linear elements for all variable fields. Additional tests indicated that the use of bi-quadratic elements for the solid and fluid displacement fields, while maintaining a bi-linear approximation for the pressure field, lead to numerical instabilities. Consequently, the guarantee of stability when using mixed-order elements in quasi-static two-field formulations cannot be extended to the three-field model – for both dCS and BT theories [18].

6 CONCLUSIONS

This work presented the derivation of a finite element model for porous media simulation using the de la Cruz and Spanos (dCS) theory. When compared to the commonly used Biot (BT) theory, the dCS model includes viscous dissipation terms, non-reciprocal solid-fluid interactions, and a micro-heterogeneity parameter. Hence, it is important to understand whether these contributions lead to any discrepancy from the BT model, and if so, under which circumstances this might happen. One-dimensional examples were used for a verification and convergence study, and for the evaluation of the impact of dCS fluid viscous dissipation terms. The verification study showed optimal convergence rates for the three-field model, and how these rates are dependent on the level of coupling between solid and fluid constituents. For the simulations considering five different solid-fluid combinations, we concluded that viscous effects are more significant for specific sets of materials, and differences appear mainly for high fluid viscosity and at high frequencies. A two-dimensional example was used to show the propagation of dif-

ferent wave types and to observe the effect of the non-reciprocal interactions introduced in the dCS framework. Variations in the parameter n lead to changes in velocity and attenuation, and the extent of these changes is also dependent on the material properties of the medium.

REFERENCES

[1] T. J. T. Spanos, *The Thermophysics of Porous Media*. Chapman & Hall, 2002.

[2] M. A. Biot, "Theory of propagation of elastic waves in a fluid-saturated porous solid - i. low-frequency range," *The Journal of the Acoustical Society of America*, vol. 28, no. 168, pp. 168–178, 1956.

[3] B. Campos and R. Gracie, "A fem for three-field u–p–η poroelasticity with nonreciprocal interactions," *International Journal for Numerical and Analytical Methods in Geomechanics*, vol. 48, no. 1, pp. 332–355, 2023.

[4] M. A. Biot, "General Theory of Three Dimensional Consolidation," *Journal of Applied Physics*, vol. 155, no. 12, pp. 155–164, 1941.

[5] J. Korsawe, G. Starke, W. Wang, and O. Kolditz, "Finite element analysis of poro-elastic consolidation in porous media: Standard and mixed approaches," *Computer Methods in Applied Mechanics and Engineering*, vol. 195, pp. 1096–1115, 2006.

[6] Z. Zong, F. Chen, X. Yin, and K. Li, "Effect of stress on wave propagation in fluid-saturated porous thermoelastic media," *Surveys in Geophysics*, vol. 44, no. 2, pp. 425–462, 2023.

[7] L. Mountassir, T. Bassidi, and H. Nounah, "Theoretical and experimental studies of the bone damage detection by the ultrasonic method," *Russian Journal of Nondestructive Testing*, vol. 57, pp. 525–540, 2021.

[8] T. M. Müller and P. N. Sahay, "Elastic potential energy in linear poroelasticity," *Geophysics*, vol. 84, no. 4, pp. W1–W20, 2019.

[9] P. N. Sahay, "On the biot slow s-wave," *Geophysics*, vol. 73, no. 4, pp. N19–N33, 2008.

[10] R. de Boer, *Theory of Porous Media: Highlights in Historical Development and Current State*. Springer-Verlag, 2000.

[11] V. De La Cruz and T. J. T. Spanos, "Seismic Wave Propagation in a Porous Medium," *Geophysics*, vol. 50, no. 10, pp. 1525–1648, 1985.

[12] V. De La Cruz and T. J. T. Spanos, "Thermomechanical coupling during seismic wave propagation in a porous medium," *Journal of Geophysical Research: Solid Earth*, vol. 94, no. B1, pp. 637–642, 1989.

[13] G. Quiroga-Goode, S. Jimenez-Hernandez, M. A. Perez-Flores, and R. Padilla-Hernandez, "Computational study of seismic waves in homogeneous dynamic porosity media with thermal and fluid relaxation: Gauging biot theory," *Journal of Geophysical Research: Solid Earth*, vol. 110, no. B7, p. B07303, 2005.

[14] P. N. Sahay, "Biot constitutive relation and porosity perturbation equation," *Geophysics*, vol. 78, no. 5, pp. L57–L67, 2013.

[15] G. Li, X. Su, and H. Pu, "An unconditionally stable and high-accuracy finite element scheme for dynamic analysis of saturated poroelastic media," *Soil Dynamics and Earthquake Engineering*, vol. 136, p. 106226, 2020.

[16] J. Liang and J. Liang, "A user-defined element for dynamic analysis of saturated porous media in abaqus," *Computers and Geotechnics*, vol. 126, p. 103693, 2020.

[17] B. Jeremić, Z. Cheng, M. Taiebat, and Y. Dafalias, "Numerical simulation of fully saturated porous materials," *International Journal for Numerical and Analytical Methods in Geomechanics*, vol. 32, no. 13, pp. 1635–1660, 2008.

[18] P. Tasiopoulou, M. Taiebat, N. Tafazzoli, and B. Jeremic, "Solution verification procedures for modeling and simulation of fully coupled porous media: static and dynamic behavior," *Coupled Systems Mechanics*, vol. 4, no. 1, pp. 67–98, 2015.

[19] N. M. Newmark, "A method of computation for structural dynamics," *Journal of the engineering mechanics division*, vol. 85, no. 3, pp. 67–94, 1959.

[20] C. Yew and P. Jogi, "The determination of biot's parameters for sandstones: Part 1: Static tests experimental procedure for determining biot's parameters for four rock specimens is presented and theoretical values of wave speeds propagating through them are compared with experimental values," *Experimental Mechanics*, vol. 18, pp. 167–172, 1978.

[21] A. Hosokawa and T. Otani, "Ultrasonic wave propagation in bovine cancellous bone," *The Journal of the Acoustical Society of America*, vol. 101, no. 1, pp. 558–562, 1997.

[22] S. Picotti, J. M. Carcione, and M. Pavan, "Seismic attenuation in antarctic firn," *The Cryosphere*, vol. 2024, no. 18, pp. 169–186, 2024.

[23] M. Kimura, "Study on the biot-stoll model for porous marine sediments," *Acoustical science and technology*, vol. 28, no. 4, pp. 230–243, 2007.